PROCEEDINGS OF THE ROYAL SOCIETY B

rspb.royalsocietypublishing.org

Research

Cite this article: Khonsari RH, Olivier J, Vigneaux P, Sanchez S, Tafforeau P, Ahlberg PE, Di Rocco F, Bresch D, Corre P, Ohazama A, Sharpe PT, Calvez V. 2013 A mathematical model for mechanotransduction at the early steps of suture formation. Proc R Soc B 280: 20122670.
http://dx.doi.org/10.1098/rspb.2012.2670

Received: 14 November 2012
Accepted: 25 February 2013

Subject Areas:
evolution, theoretical biology, developmental biology

Keywords:
sutural bone growth, mechanical instability, partial differential equation, synchrotron microtomography, mechanotransduction

Authors for correspondence:
R. H. Khonsari
e-mail: roman.khonsari@kcl.ac.uk
J. Olivier
e-mail: julien.olivier@acmac.uoc.gr

Electronic supplementary material is available at http://dx.doi.org/10.1098/rspb.2012.2670 or via http://rspb.royalsocietypublishing.org.

Royal Society Publishing
Informing the science of the future

A mathematical model for mechanotransduction at the early steps of suture formation

R. H. Khonsari[1,2], J. Olivier[3], P. Vigneaux[4], S. Sanchez[5], P. Tafforeau[5], P. E. Ahlberg[6], F. Di Rocco[7], D. Bresch[8], P. Corre[2], A. Ohazama[1], P. T. Sharpe[1] and V. Calvez[4]

[1]Department of Craniofacial Development and Stem Cell Research, Comprehensive Biomedical Research, Dental Institute, King's College London, London, UK
[2]Service de Chirurgie maxillofaciale, Centre Hospitalier Universitaire, Nantes, France
[3]Archimedes Center for Modeling, Analysis and Computation (ACMAC), Heraklion, Crete, Greece
[4]Unité de Mathématiques Pures et Appliquées, École Normale Supérieure de Lyon, CNRS UMR, 5669 Lyon, France
[5]European Synchrotron Radiation Facility (ESRF), Grenoble, France
[6]Evolutionary Biology Centre, Uppsala University, Uppsala, Sweden
[7]Department of Pediatric Neurosurgery, Hôpital Necker-Enfants-Malades, Paris, France
[8]Laboratoire de Mathématiques (LAMA), Université de Savoie, CNRS UMR, 5127 Chambéry, France

Growth and patterning of craniofacial sutures is subjected to the effects of mechanical stress. Mechanotransduction processes occurring at the margins of the sutures are not precisely understood. Here, we propose a simple theoretical model based on the orientation of collagen fibres within the suture in response to local stress. We demonstrate that fibre alignment generates an instability leading to the emergence of interdigitations. We confirm the appearance of this instability both analytically and numerically. To support our model, we use histology and synchrotron X-ray microtomography and reveal the fine structure of fibres within the sutural mesenchyme and their insertion into the bone. Furthermore, using a mouse model with impaired mechanotransduction, we show that the architecture of sutures is disturbed when forces are not interpreted properly. Finally, by studying the structure of sutures in the mouse, the rat, an actinopterygian (*Polypterus bichir*) and a placoderm (*Compagopiscis croucheri*), we show that bone deposition patterns during dermal bone growth are conserved within jawed vertebrates. In total, these results support the role of mechanical constraints in the growth and patterning of craniofacial sutures, a process that was probably effective at the emergence of gnathostomes, and provide new directions for the understanding of normal and pathological suture fusion.

1. Introduction

Craniofacial bones are connected by sutures, which act as joints, absorb shocks during impacts [1] and work as intramembranous bone growth sites [2]. Even though sutures seem to have little functional roles when compared with the long bone joints such as knees or wrists, they are major actors in the morphogenesis of the head of newborns. In fact, after birth, most skull growth is owing to the action of sutures [2], and clinicians are well aware that abnormal suture maintenance and premature fusion can lead to remarked skull deformations known as craniosynostoses [3].

This study aims at a better understanding of the interactions between external mechanical forces and bone deposition inside sutures. The fact that bone deposition occurring on the borders of the sutures is subjected to the influence of external mechanical stimuli has been demonstrated in experimental systems [4]. Nevertheless, the way external mechanical information is transmitted to cells inside sutures is not explained in detail, even though this point is of interest in the understanding of the origins of craniosynostoses. Here, we used a theoretical approach in order to explore mechanotransduction processes at the early stages of suture formation.

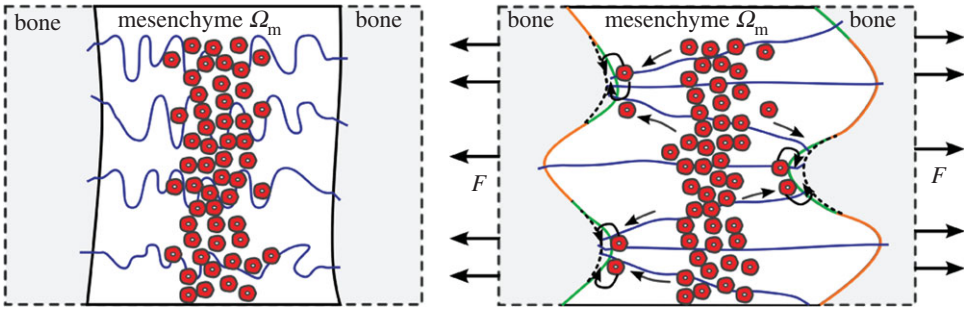

Figure 1. Schematic of the different components of the model. At rest, the borders of the suture are nearly parallel; the osteogenic cells of the mesenchyme are located at the centre of the suture (red; compare with electronic supplementary material, figure S3) and the collagen fibres have no preferential orientation (blue). When submitted to a traction *F*, the suture witnesses several transformations: the collagen fibres self-organize into a specific pattern (compare with figure 2), the osteogenic cells migrate towards the borders of the suture (compare with electronic supplementary material, figure S3) and preferentially deposit bone in regions that eventually become the convexities (green), as opposed to concavities (orange) where no bone deposition occurs. This process leads to the formation of interdigitations.

Sutures are delimited by two bony borders and contain an undifferentiated, osteogenic, mesenchyme [5] (figure 1). The two borders of the suture are interconnected by a dense network of collagen fibres [6–8]. During growth, most sutures, such as the skull vault sutures of mammals, progressively develop a striking, interdigitated pattern [9]. From a morphological point of view, it is known that sutures interdigitate in the first weeks after birth [10]. It is also known that bone deposition in sutures mainly occurs at the convexities of the interdigitations [7,11], whereas the concavities are subjected to resorption [12]. Furthermore, collagen fibres within the mesenchyme radiate in a fan-shaped pattern from the convexities to the concavities in the interdigitated areas [4,13]. The conservation of these morphological characteristics in theoretical models can be used to check whether the initial hypotheses are biologically sound.

In this perspective, the emergence of interdigitations has already been modelled. Miura *et al.* [10] proposed a chemical reaction–diffusion system developing a Turing instability [14,15]. In this study, a specific choice in the biochemical reaction term led to the formation of labyrinthic patterns that resembled sutures. Nevertheless, even though morphogens are determinants of embryonic suture development [2,9], mechanical forces have to be taken into account in order to explain how sutures grow after birth and develop their peculiar architecture [2]. Another morphogenetic model for sutures has been recently proposed [16] and involved 'viscous fingering' phenomena similar to those occurring between two immiscible liquids with different viscosities. Here, again, the model reproduces the evolution of the interdigitations.

We propose an alternative approach based on a biomechanical model. Our approach is complementary to the chemical system studied by Miura *et al.* [10]. Our model is based on simple and generic processes that are known to occur *in vivo*. The couplings between these processes produce an instability that can be linked to the onset of digitations. We based the formalism of the model on three biomechanical processes. First, collagen fibres within the suture mesenchyme were instructed to orientate following local mechanical information such as the direction and the intensity of the principal stresses [17,18]. Second, the mesenchymal cells were programmed to migrate following the average direction of fibres (haptotaxis directed by mechanical information [19]). Last, bone deposition owing to the migrating mesenchymal cells drove the motion of the interface between the initial bony border and the mesenchyme [6]. More precisely, mesenchymal cells were forced to differentiate into osteoblasts when reaching the bony border of the tissue. The local variations in the density of the migrating cells produced different ossification velocities along the border of the suture and induced interdigitated patterns. This system led to the appearance of a previously unknown kind of instability.

We studied the distribution of collagen fibres within the sutural mesenchyme, osteocyte populations, peri-sutural vascular channels and bone growth lines using histology and high-resolution synchrotron microtomography on mice, rats and on two basal gnathostomes (actinopterygian *Polypterus bichir* and placoderm *Compagopiscis croucheri*). Morphologically, the data collected on these various gnathostomes matched the results of the model. We described the distribution of neural-crest-derived osteogenic cells within the mouse adult sutural mesenchyme, using a *R26R;Wnt1-Cre* compound and illustrated the importance of mechanical forces in suture patterning using a *Pkd2*$^{fl/fl}$*;Wnt1-Cre* mouse with defective mechanotransduction.

In brief, the model we propose is derived from generic processes: linear elasticity, fibre orientation and transport-diffusion. We excluded any initial geometrical hypothesis on the structure of the borders of the sutures and on the mesenchyme. By taking into account the reorganization of collagen fibres subjected to mechanical stress [17], we analysed the emergence of interdigitations through cell movements in the sutural mesenchyme. The emerging pattern we found was consistent with biological data. This model is, to our knowledge, the first attempt to build a theoretical relationship between external mechanical conditions (brain growth, action of masticatory muscles on the borders of the suture) and cellular events resulting in sutural bone formation.

2. Material and methods

(a) Mouse data

Pkd2-floxed mice were bred as already described [20]. *R26R* and *Wnt1-Cre* mice were produced as previously described [21,22]. All animal experiments were approved by the UK Home Office. Timed matings were set up such that the noon of the day on which vaginal plugs were detected was considered E0.5. Collection of embryonic and neonatal tissue was carried out according to the Home office's schedule one specification. Heads of mouse embryos were dissected, fixed in 4 per cent paraformaldehyde at 4°C, decalcified in Morse solution and dehydrated in

Table 1. Biological parameters used in the numerical simulations.

parameter	value	reference
width of the suture	0.5–1 mm	direct measurement
duration of constraint application	30 days	direct measurement
traction (F)	100 kPa	Jasinoski *et al.* [19]
Young modulus for bone (E_b)	6000 Mpa	Jasinoski *et al.* [19]
Young modulus for mesenchyme (E_m)	50 MPa	Jasinoski *et al.* [19]
Poisson's ratio bone (ν_b)	0.27	Jasinoski *et al.* [19]
Poisson's ratio mesenchyme (ν_m)	0.30	Jasinoski *et al.* [19]
mesenchymal cell density	10^3 per mm^2	Peptan *et al.* [24]
haptotaxis intensity (χ)	1 mm per day	ad hoc
mesenchymal cells diffusion (D)	0.1 mm^2 per day	Murray [18]
speed of deposition of bone on the border (v_0)	0.1 mm per day	Murray [18]

ascending ethanol solutions before paraffin embedding. Samples were sectioned at 7–12 µm, using a Leica RM2245 microtome. Picrosirius staining was used for morphological studies. Sections were viewed in light-field, using a Zeiss microscope (axioskope 2 plus) and captured with an AxioCam HRC (Zeiss), using Axiovision software. Transgenic mice carrying a LacZ reporter were processed through a LacZ staining protocol with eosin counterstaining prior to histology analysis.

(b) Synchrotron X-ray microtomography

The following samples were imaged at the European Synchrotron Radiation Facility, Grenoble, at the beamline ID19: *C. croucheri* (interolateral and anterior ventral plates) from the National History Museum, London: BMNH P 51007, *P. bichir* (parietal sutures in an adult and a juvenile specimen) from the Museum of Evolution at Uppsala University: PMU 25738, 25739, *Rattus rattus* from a personal collection, *Mus musculus* (CD1 background) from King's College London. Experiments were carried out using either a monochromatic beam or a pink beam according to the nature of the samples (see the electronic supplementary material, tables S1 and S2 in file S2). All scans were carried out with a FreLoN 2K14 CCD camera (fast readout low noise) coupled to a Gadolinium oxysulphide crystal of 40 µm thickness (Gadox40) or a gadolinium gallium garnet crystal of 10 µm thickness (GGG10) scintillator, depending on the voxel size.

(c) Mathematical methods

The model presented in §2*c*(i) is studied mathematically using two approaches: (i) analysis of the linear stability of a planar interface, and (ii) numerical solution of the full model and investigation of its patterning abilities.

(i) The model: mathematical formalism for mechanotransduction in skull vault sutures

The mathematical formalism for mechanotransduction in sutures was designed in order to fulfil three objectives:

(1) describe the mechanical behaviour of sutures;
(2) render both the cellular motion within sutures and the sensitivity of these cell movements to the mechanical environment; and
(3) simulate ossification and its effects on the growing sutures.

From a mechanical point of view, a craniofacial suture is a medium consisting of the whole plane Ω divided into two subdomains representing the bone Ω_b and the mesenchyme Ω_m. The border of sutures is defined as $\Gamma_{bm} = \partial\Omega_b \cap \partial\Omega_m$.

We chose to model biological processes occurring in the sutures at the continuous scale, thus discarding, for instance, every individual cell behaviour. With this assumption, the mechanical aspects of the problem were easier to render and we could apply the standard theory of continuum mechanics. Furthermore, because we were interested in the emergence of patterns at a local level, we discarded the effect of depth in the skull vault as well as curvature, and considered an infinite medium, thus neglecting far-field effects.

Even though the mechanical behaviour of sutures is viscoelastic and nonlinear in response to external parameters such as tension, compression or shearing [23], we decided to restrict our description to a linear isotropic elastic behaviour, for simplification purposes. Viscoelastic modelling would have led to difficulties in implementing experimental values into the numerical simulations. Furthermore, as we will show further, the elastic model was sufficient to describe the emergence of an instability, which could then be characterized analytically. The analytical solution for the emergence of the instability would have been more difficult to compute in a viscoelastic model. Finally, our model focused on the onset of suture patterning. These processes take place at a biological time when we supposed that nonlinearities and complex behaviours did not have to be taken into account.

In brief, knowing the difference of rigidity between bone and mesenchyme, we used the classical equations of elasticity, which related the stress tensor σ to the displacement u through the Lamé equations:

$$\left.\begin{aligned} &-\mathrm{div}\,\sigma = 0,\ x \in \Omega \ \text{ with } \sigma n = F \text{ (resp. } 0) \text{ on the vertical} \\ &\text{(resp. horizontal) boundary of } \Omega, \\ \text{and} \quad &\sigma(u) = \frac{E(x)\nu}{(1+\nu)(1-\nu)}(\mathrm{div}\,u)\mathbf{Id} + \frac{E(x)}{2(1+\nu)}(\nabla u + (\nabla u)^t), \end{aligned}\right\} \tag{2.1}$$

where **Id** stood for the 2×2 identity matrix. In the Lamé equations, $E(x)$ stood for the Young modulus of the medium ($E(x) = E_b$ for bone and $E(x) = E_m$ for mesenchyme). To account for the difference of rigidity, we assumed $E_b \gg E_m$. The coefficient ν was the classical Poisson's ratio, assumed to be the same in both subdomains. In fact, Poisson's ratios for bone and mesenchyme are very close (table 1), and we chose their average as a common value (see the electronic supplementary material, file S1 for the discussion of this choice). Finally, the effects of the external environment (restricted to an outer traction $F > 0$, see figure 1) were modelled as boundary conditions.

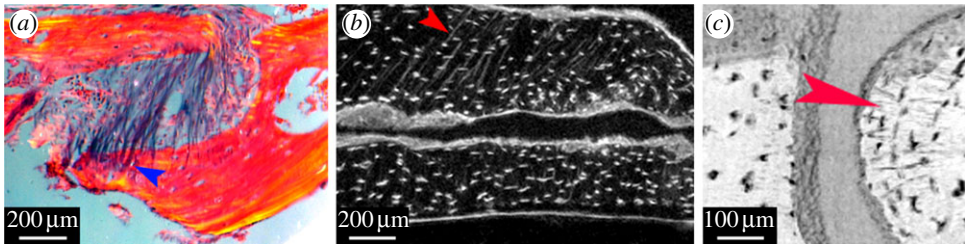

Figure 2. Collagen fibres in skull vault sutures. (*a*) Sharpey's fibres within the coronal suture of an adult mouse (arrowhead: insertion point of the fibres in the lower border); picrosirius staining. (*b*) Sharpey's fibres within the borders of the coronal suture of a P20 wild-type mouse (arrowhead); lateral view; virtual section obtained by computing the standard deviation of the signal over 20 sections acquired by synchrotron X-ray microtomography with a 1.36 voxel size. (*c*) Virtual section from the same dataset in upper view, obtained by computing the minimal signal value over 20 sections; radiating Sharpey's fibres in the convex borders of the suture (arrowhead).

In order to describe cellular motion in the mesenchyme, we considered two mesenchymal components: the osteogenic cells and the fibres (figure 2; electronic supplementary material, figures S2 and S3). Collagen fibres were evenly distributed in the mesenchyme and defined the directions along which the osteogenic cell could move preferentially. Fibres were modelled as a vector field $\mathbf{e}$.

The fibres were expected to orientate according to local mechanical stresses [17,18]. We denoted the two eigenmodes of the stress tensor σ by (σ_1, σ_2) along the directions ($\mathbf{e}_1$, $\mathbf{e}_2$) ($\mathbf{e}_1$ and $\mathbf{e}_2$ were normalized). We assumed, without loss of generality, that $\sigma_1 \geq \sigma_2$.

According to Sherratt *et al*. [17] and Murray [18], the main orientation of fibres is given by

$$\begin{cases} \mathbf{e} = G(\sigma_1\sigma_2 - 1)\mathbf{e}_1, & \text{if } 0 \leq \sigma_2 \leq \sigma_1, \\ \mathbf{e} = \mathbf{e}_1, & \text{if } \sigma_2 < 0 < \sigma_1, \\ \mathbf{e} = 0, & \text{if } \sigma_2 \leq \sigma_1 \leq 0. \end{cases} \tag{2.2}$$

This was derived from the following rules (figure 1):

(1) fibre rearrangement was active only under tension ($\sigma_1 > 0$);
(2) when σ_1 and σ_2 were both positive, the two effects were competing, and the resulting orientation depended on the anisotropy ratio σ_1/σ_2 through the increasing function G that took values between 0, when $\sigma_1 = \sigma_2$ (*isotropic case*) and 1, when $\sigma_1 \gg \sigma_2$ (*anisotropic case*); the precise shape of the function G did not play an important role; and
(3) when σ_1 and σ_2 had opposite signs the fibres orientated in the direction of the positive eigenmode.

Of note, by defining the sign of eigenvectors, we assumed $\mathbf{e}_1$ (and hence $\mathbf{e}$) to point 'from left to right', as in figure 1.

The equation monitoring the density of the osteogenic cell ρ had the following characteristics:

— *diffusion*: the motion of the osteogenic cells was supposed to be anisotropic, as we expected diffusion to be greater along the fibres; motion had no preferential direction along the fibres; and
— *haptotaxis*: the motion of the osteogenic cells was assumed to follow the fibres and to be directed towards the closest border of the suture.

We assumed that cell movements were much faster than the speed of the ossification front, so that the motion of the cells was driven by the following stationary diffusion-transport equation:

$$\nabla \cdot (\underbrace{-\mathbf{D}(\mathbf{e})\nabla\rho}_{\text{diffusion}} + \underbrace{\rho\mathbf{h}(\mathbf{e})}_{\text{haptotaxis}}) = 0, \quad x \in \Omega_m, \quad t > 0, \tag{2.3}$$

where $\mathbf{D}(\mathbf{e})$ is the anisotropic diffusion tensor, and $\mathbf{h}(\mathbf{e})$ is the biased speed of motion.

We further considered both these quantities. In the model, fibres defined the bias direction, so that the haptotaxis field $\mathbf{h}$ was aligned with the main orientation of fibres, which meant that $\mathbf{h}$ was parallel to $\mathbf{e}$:

$$\mathbf{h}(x) = p(x)\mathbf{e}(x). \tag{2.4}$$

The factor p took into account polarizing chemical signals such as fibroblast growth factor 2 (FGF2) [25] produced by the osteocytes of the sutural borders. These signals reached the point x of the domain and were used to indicate the closest border to the point x. As $\mathbf{e}$ always pointed to the right, we could define p as

$$p(x) = \begin{cases} -\chi, & \text{if } x \text{ is closer to the left border,} \\ \chi, & \text{if } x \text{ is closer to the right border,} \end{cases}$$

where χ is the typical bias speed.

The anisotropic tensor was locally defined by $\mathbf{D} = (D_1/\|\mathbf{e}\|^2)\mathbf{e} \otimes \mathbf{e} + (D_2/\|\mathbf{e}^\perp\|^2)\mathbf{e}^\perp \otimes \mathbf{e}^\perp$ with $D_1 \geq D_2$ (preferential diffusion in the direction of the fibres rather than in the transverse direction $\mathbf{e}^\perp$).

The field $\mathbf{h}$ resulted from the fibre orientation pattern. We assumed that the suture mesenchyme had a fast renewal rate in order to compensate for the loss of cells owing to migration and ossification. We included this constraint in the model by imposing that the total number of mesenchymal cells would remain constant. More precisely, we assumed a constant supply of cells in the suture, relying on proliferation factors such as fibroblast growth factor receptor 2 (FGFR2) interacting with the diffusion morphogen FGF2 [26]. Cellular differentiation occurred at the borders of the suture by the action of factors such as FGFR1 interacting with the same diffusion morphogen FGF2 [26]. The bone was produced by the mesenchymal cells in the immediate vicinity of the borders of the suture [27].

The interface was supposed to move because of bone deposition and external mechanical traction. We modelled bone deposition as a motion of the interface in the orthogonal direction towards the centre of the suture:

$$\mathbf{v}_{\text{ossi}} = v_0 \frac{\rho - \langle\rho\rangle}{\langle\rho\rangle}\mathbf{n}, \tag{2.5}$$

where v_0 is the characteristic speed of ossification (or bone deposition), $\langle\rho\rangle$ is the average of ρ and $\mathbf{n}$ is the normal vector to the interface. Intuitively, ossification speed is proportional to the relative amount of cells close to the suture border. We choose the relative amount $\rho - \langle\rho\rangle$ instead of the absolute amount ρ to maintain a widely opened suture during the time range of the process.

(ii) Linear stability analysis

Using previously described methods [28], we investigated the linear stability of a configuration with initially parallel sutural borders. For this, we analysed the amplification or the damping of small perturbations applied to a planar configuration $\{x = x_0\}$. We thus started the analysis by assuming that the initial interface was perturbed using a small sinusoidal wave with amplitude

$\varepsilon \ll 1$ and frequency mode k (see the electronic supplementary material, figure S1, left):

$$x = x_0 + \varepsilon \sin(ky).$$

We then screened for a solution (evolving with time t) of the form:

$$x(t) = x_0 + \varepsilon e^{s(k)t} \sin(ky), \tag{2.6}$$

where s is a function to be determined through the derivation of the so-called *dispersion relation* (see the electronic supplementary material, file S1 for further details).

Consequently, when $s(k) > 0$, the oscillations were amplified. We defined this state as unstable. When $s(k) < 0$, the initial oscillations were damped, and the interface became more and more straight.

As mentioned earlier, we considered the case where the Young modulus E was constant in each of the two subdomains (mesenchyme and bone tissue). We also considered that $\nu_m = \nu_b$. Given that these two values are close (table 1), we used their mean. In order to simplify the calculations, we opted for an isotropic diffusion matrix (D being the diffusion coefficient), namely $\mathbf{D} = D\mathbf{Id}$. We put the anisotropy effect on the haptotaxis field $\mathbf{h}$. The ratio of anisotropy is denoted by

$$\alpha = \sqrt{\frac{D_2}{D_1}} \leq 1, \tag{2.7}$$

where $\alpha = 1$ in the isotropic case. The details of the computations are given in the electronic supplementary material, file S1.

As a matter of fact, in the numerical framework, ε can be seen as a numerical roughness of the interface (see the electronic supplementary material, figure S1, right).

Such a linear stability analysis provides insights into the model presented in §2*c*(i) as well as into the results of the numerical simulations based on this model (see further in the text). Choosing an initial sine perturbation is not a restrictive hypothesis, and the stability results we obtained can be generalized to any other type of initial perturbation, even to a random shape perturbation whose extracted amplitude and frequency would be of order ε and k, respectively. The small errors inherent to any computer simulations (round-off error or moving meshes for instance) are the numerical counterpart of the analytical sine perturbation considered in the linear stability analysis performed in the electronic supplementary material, file S1.

(iii) Numerical methods for simulations

In order to explore fully the model, we solved it numerically according to the principles exposed in §2*c*(i). Namely, the numerical analysis algorithm could be summarized as follows:

(1) the elasticity problem (2.1) was solved for u, from which we deduced the principal stresses;
(2) we computed the haptotaxis field $\mathbf{h}(\mathbf{e})$ through (2.2) and (2.4);
(3) the diffusion-transport problem (2.3) was solved for ρ, from which we determined the ossification speed $\mathbf{v}_{ossi}$ *via* (2.5);
(4) the motion of the interface Γ_{bm} between bone and mesenchyme was computed, thanks to $\mathbf{v}_{ossi}$; and
(5) we iterated steps (1)–(4) in order to obtain the time evolution of the suture.

The interface Γ_{bm} is defined as

$$\Gamma_{bm}(t) = \{x : \phi(t, x) = 0\},$$

where ϕ is a so-called *level set function*, which defines the interface implicitly. Indeed, we used a *level-set* method [29] in order to describe the movement of the interface according to the transport induced by the speed $\mathbf{v}_{ossi}$. This is performed by solving the following usual equation:

$$\partial_t \phi + \mathbf{v}_{ossi} \cdot \nabla \phi = 0.$$

The implementation of the numerical resolution was carried out by using the public domain finite-element library FreeFem++ (all the above equations were solved by the finite-element method, see the electronic supplementary material, file S1 for details). The biological parameters of the model were extracted from the literature on suture biology (table 1).

3. Results

(a) Microscopic structure of craniofacial sutures

Histology and high-resolution imaging allowed us to obtain relevant parameters of sutural anatomy. We considered sutures as structures made of two rigid bony borders connected by a network of collagen fibres. In between the two borders, the sutural mesenchyme contained a population of osteogenic cells. Using standard histology, we visualized the insertion of Sharpey's fibres into the borders of the suture (figure 2). Synchrotron X-ray microtomography confirmed the presence of Sharpey's fibres within peri-sutural bone. Virtual histological sections showed that these fibres were organized in a fan-shaped pattern in the convexities of the sutures. This pattern had been hypothesized [19] but never, to our knowledge, visualized previously. Further microscopic information provided by high-resolution imaging was in favour of a specific pattern of bone deposition along the sutures: osteocytes, which are the osteogenic cells, were concentrated in the convexities of the peri-sutural bone, whereas the concavities showed indirect signs of osteoclastic resorption (see the electronic supplementary material, figure S2). Finally, using a *R26R-Wnt1-Cre* mouse in order to track neural-crest-derived cells, we showed that adult sutures contained a population of such cells in the core of their mesenchyme, that were progressively migrating towards the bony borders and integrating into the peri-sutural bone (see the electronic supplementary material, figure S3).

(b) Mechanically driven morphogenesis of interdigitations

We first investigated the linear stability of the parallel border configuration when the suture was submitted to mechanical traction. We derived the following dispersion relation, giving the stability exponent s as a function of the perturbation mode k. We established the following formula, involving reduced parameters of interest. Thus, we could discuss the influence of each parameter on stability:

$$s(k) = v_0 k_0 \mathcal{S}\left(\frac{k}{k_0}; \alpha, \frac{E_m}{E_b}, \nu, \mathcal{G}\right), \tag{3.1}$$

where we have set the characteristic parameters

$$k_0 = \frac{\chi}{D} G\left(\frac{1}{\nu} - 2\right) \quad \text{and} \quad \mathcal{G} = \frac{G'(1/\nu - 2)}{G(1/\nu - 2)},$$

where G' is standing for the derivative function of G and $\mathcal{S}$ is a function detailed in the electronic supplementary material, file S1. The factor v_0 denoted the characteristic speed of ossification (or bone deposition) as defined in equation (2.5). The ratio χ/D denoted the ability of mesenchymal cells to respond to haptotactic signalling. These factors had no influence on the sign of $s(k)$. The sign of $s(k)$ depended only on the mechanical aspects of the model, namely the ratio of Young moduli and common Poisson's ratio as well as the function G. One crucial result of the stability analysis was that G established a link between the mechanical characteristics of the tissues (e.g. the Poisson's ratio ν) and the local orientation of the fibres.

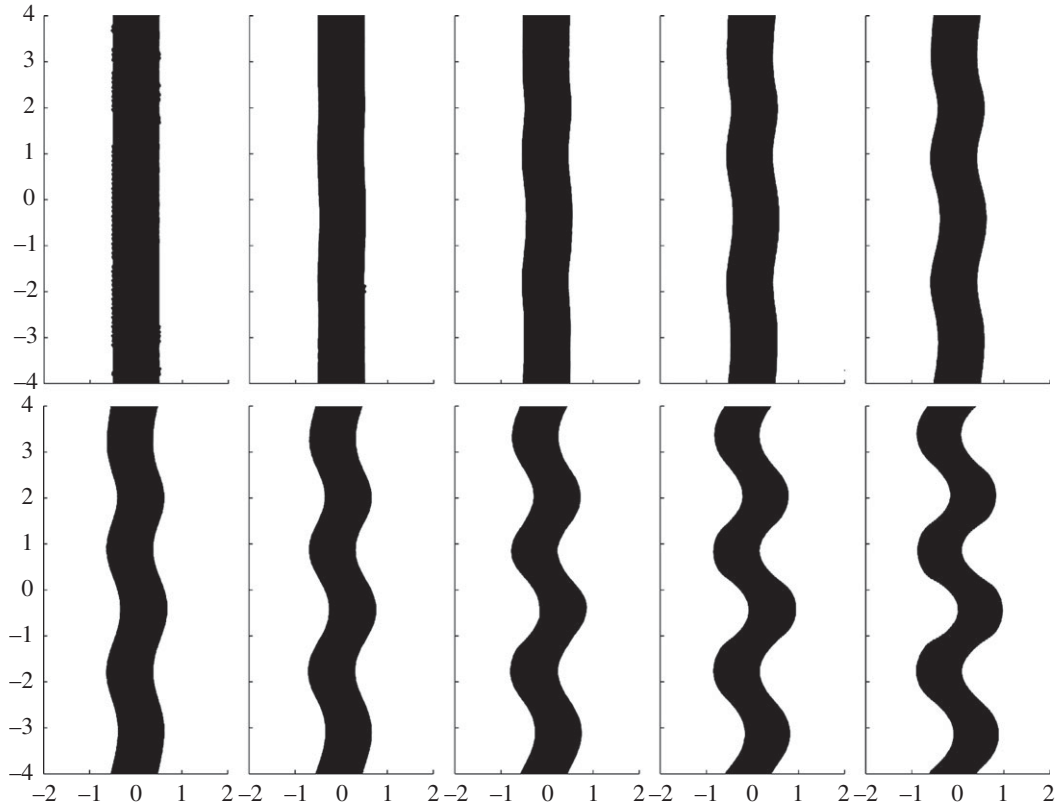

Figure 3. Onset of the instability. Snapshots of the interface. Starting from a straight interface, the suture evolved towards a sinusoidal shape resembling the interdigitations of real sutures. The simulation spanned over 30 days. Size of each snapshot: 4 mm (width) × 8 mm (height); see also figure 4*a* for a closer view.

The relation (3.1) can be greatly simplified when the Young moduli (respectively for the bone and for the mesenchyme) are very different, namely $E_b \gg E_m$, and when the highly oscillatory limit $k \gg k_0$ is considered. This limit is informative as it is expected from some graphical representations of (3.1) that $s(k)$ is decaying for large k/k_0. A positive limit ensures that an interesting instability will emerge at an intermediate mode k. We refer to the electronic supplementary material, file S1 for further discussion of the dispersion relation (3.1) in other regimes. We obtained:

$$\lim_{\substack{k\gg k_0 \\ E_b \gg E_m}} \mathcal{S}\left(\frac{k}{k_0}; \alpha, \frac{E_m}{E_b}, \nu, \mathcal{G}\right) = \left(\frac{1}{4} - \alpha + \alpha \frac{1-2\nu}{4\nu^2(3-4\nu)}\mathcal{G}\right). \quad (3.2)$$

Using the basic properties of the function G (positive and increasing), we knew that $\mathcal{G}$ was a positive quantity. Because $-1 < \nu < \frac{1}{2}$, we noticed that anisotropic diffusion along the fibres enhanced instability as the right-hand side of (3.2) was necessarily positive when α was lower than $\frac{1}{4}$. Interestingly, when α was greater than $\frac{1}{4}$, as it would be the case if we considered an isotropic diffusion of the mesenchymal cells, the ratio $\mathcal{G} = G'/G$ controlled the sign of $s(k)$ for $k \gg k_0$. When this ratio was large, an instability was more likely to grow from a planar configuration. This could be interpreted as follows. For a large $\mathcal{G}$ ratio—meaning that the function log G was stiff—the mean orientation of the fibres was sensitive to variations in the local anisotropy of the stress tensor σ_1/σ_2.

In brief, according to the asymptotic dispersion relation (3.2), the growth of instabilities depended linearly upon cellular features (speed of bone differentiation, haptotaxis), and nonlinearly upon biomechanical aspects (tissue elasticity, mechanotransduction of collagen fibres). Furthermore, mechanical features only, and not cellular features, determined whether an instability could arise or not.

Using biological parameters (table 1), the analytical study predicted an instability with a characteristic wavelength ($\lambda_0 = 2\pi/k_0$) of order $\lambda_0 \approx 1$ mm. Numerical simulations confirmed this prediction: starting from parallel borders, the simulation evolved in a similar way as sutures do in the first months after birth by forming interdigitations (figure 3). The regular aspect of the sutures we found corresponded to the aspect of the sutures during the first steps of their interdigitations [10]. We found that under mechanical stress in tension, randomly distributed collagen fibres spanning across the suture spontaneously organized into a fan-shaped orientation. As a result of this self-organization process, the bone regions with the highest concentration in fibre insertions were the regions that finite-element analysis identified as locally subjected to the highest level of mechanical stress (figure 4*b*,*c*). This fan-shaped pattern of the orientation of collagen fibres in the borders of the bone was also observed in real sutures, as revealed by high-resolution synchrotron microtomography (figure 2).

The stability analysis of the model demonstrated that our set of initial hypotheses were sufficient to account for several fundamental characteristics of skull vault sutures via self-organization processes: (i) formation of interdigitations, (ii) spontaneous arrangement of collagen fibres in a biologically relevant pattern, and (iii) biologically realistic distribution of bone deposition regions (that is in convexities).

(c) Abnormal mechanotransduction disturbs the architecture of the collagen fibres in the mesenchyme

We hypothesized that the information about external forces was transmitted to the suture via the orientation of the collagen fibres [17,18]. In order to illustrate the role of mechanotransduction

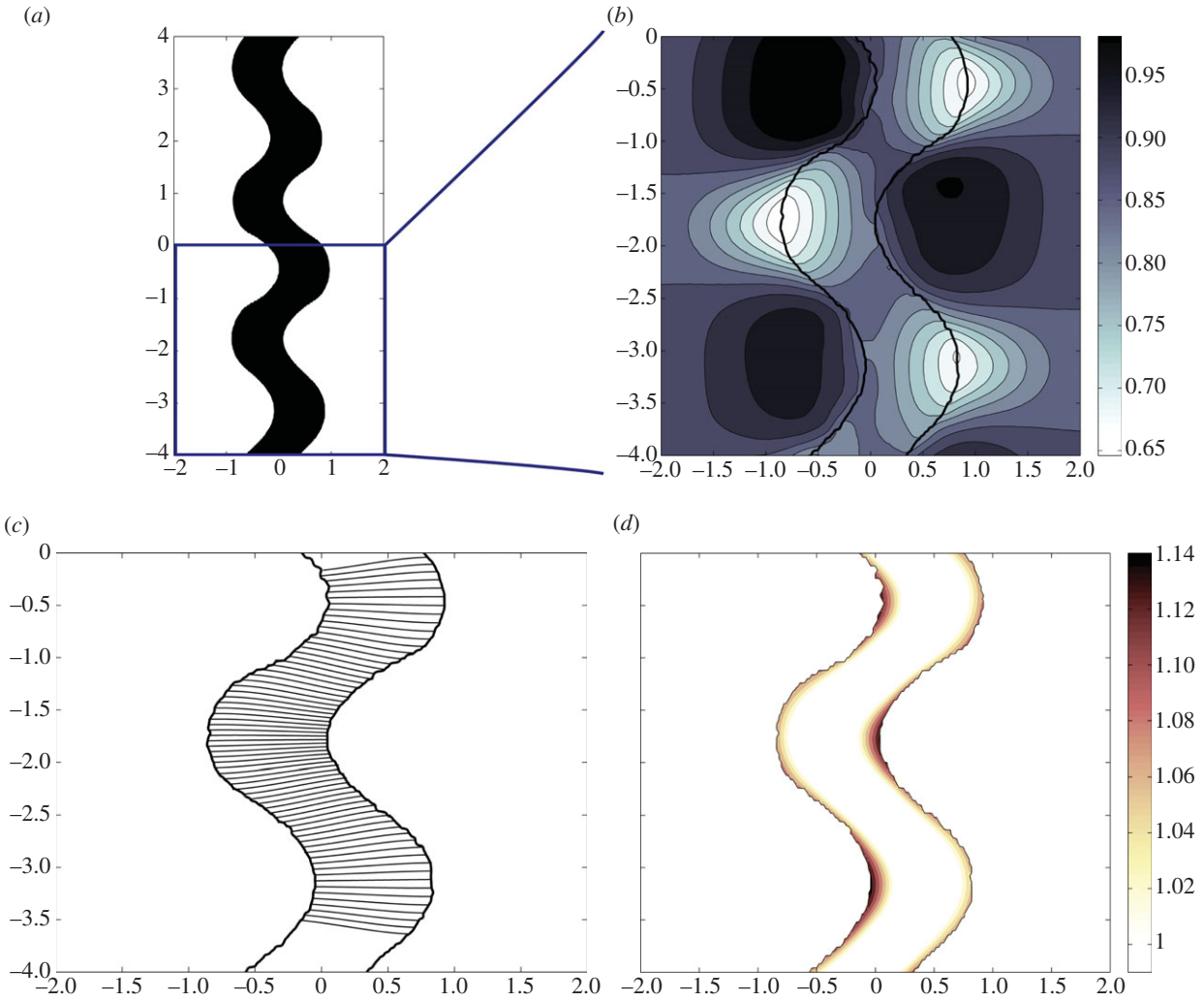

Figure 4. Biomechanical features of the instability. (*a*) Last snapshot from figure 3 showing the aspect of the simulation after 30 days. The boxed zone is enlarged in (*b–d*). (*b*) Principal stress σ_1 (MPa). The convexities were the areas subjected to the highest levels of stress. (*c*) Mean orientation of fibres (contour lines of the local vector field) in the mesenchyme: fan-shaped insertion in the convexities mimicking the insertion pattern of Sharpey's fibres in real sutures (figure 2). (*d*) Mesenchymal cell density ρ (non-dimensional unit) highlighting the pattern of bone deposition. The ossification speed was higher in the convex areas as a result of the distribution of collagen fibres. Length scales in millimetres. These three snapshots in (*b–d*) were all taken at day 30.

in suture patterning, we used a mouse strain with a conditional knockout of *Pkd2* in neural crest cells (*Pkd2*$^{fl/fl}$;*Wnt1-Cre*). Pkd1 and Pkd2 form a transmembrane heterodimer working as a calcium channel activated by the bending of primary cilia and are expressed by osteoprogenitor cells within sutures [13,30]. It is known that the lack of *Pkd1* leads to abnormal bone deposition patterns in response to external mechanical stress in mice [13,30]. Here, we show that in the fronto-maxillary suture of *Pkd2*$^{fl/fl}$;*Wnt1-Cre* mice, the lack of *Pkd2*, and thus putative defective mechanotransduction, led to a failure of suture patterning and to abnormal collagen fibre disposition across the suture (figure 5*a*,*b*). In fact, in transgenic mice, the distinctive interdigitations observed in the wild-type were lost, and the fan-shaped insertion of Sharpey's fibres within the borders was not observed (figure 5).

(d) Bone deposition in the convexities of sutures is an ancestral vertebrate character

In order to verify if the bone deposition mechanisms we studied in mammals are a general feature across other vertebrates, we first confirmed the presence of interdigitations and radiating fibres in a species close to the mouse, the rat, *R. rattus*. Interdigitations similar to those observed in mice were found in the rat (see the electronic supplementary material, figure S4). Sharpey's fibres were observed in both the sutural space (see the electronic supplementary material, figure S4*b*) and within the peri-sutural bone (see the electronic supplementary material, figure S4*c*). Next, in order to extend the conclusions of our model to extant vertebrates, we examined the structure of the sutures in a basal bony fish, the actinopterygian *P. bichir*. In this species, using high-resolution imaging, we showed the progressive complexification of the suture pattern (see the electronic supplementary material, figure S5) and the presence of denser network of blood vessels surrounding the convexities of the interdigitations (see the electronic supplementary material, figure S5, red arrow). Finally, in order to confirm the ancestral nature of the mechanisms reproduced by our model for all gnathostomes, we examined the sutures between two dermal bones (interolateral and anterior ventrolateral plates) of a placoderm fish, *C. croucheri* [31]. Placoderms are an extinct group of armoured fish-like basal gnathostomes. They form the oldest group where dermal bones and sutures can be related to the tissues observed in more derived groups

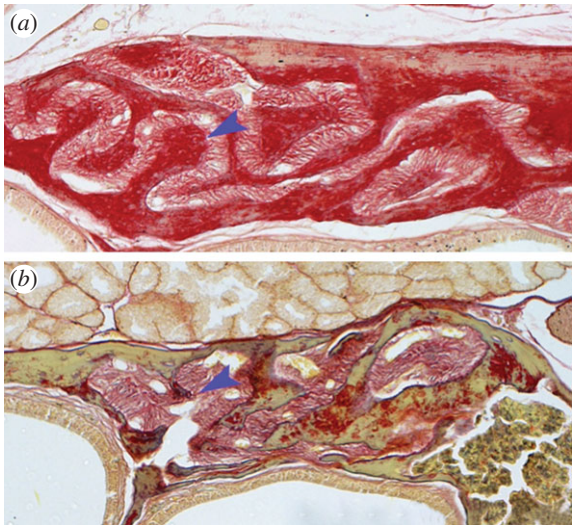

Figure 5. (*a*,*b*) Fronto-maxillary suture in adult wild-type (*a*) CD1 and (*b*) *Pkd2*$^{fl/fl}$; *Wnt1-Cre* mice; picrosirius staining; the absence of a gene involved in mechanotransduction leads to abnormal suture patterning and wrong collagen fibre insertions (arrowheads); the bone is globally depleted in collagen.

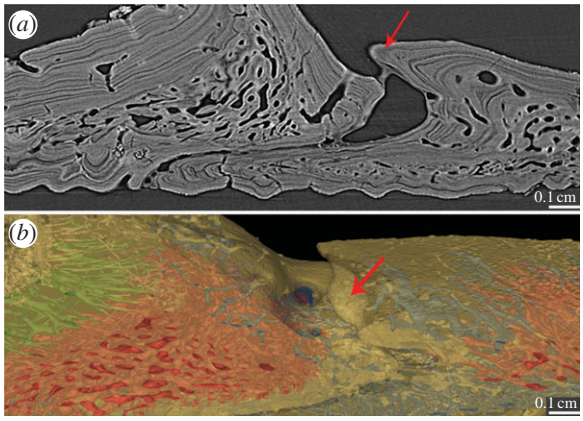

Figure 6. Pattern of sutural bone deposition in a basal extinct gnathostome. (*a*) Bone deposition in the convexities of a suture in the placoderm *Compagopiscis croucheri* (red arrow) was faster than on the confronting concavities of the same suture, as shown by the larger distance between growth lines in the latter; virtual section obtained by summing 20 sections from synchrotron X-ray microtomography data with a 5.05 voxel size. (*b*) Three-dimensional reconstruction of the same suture. Convexities (red arrow), which are putative regions with fast bone deposition, did not have a dense vascular network when compared with the opposite concave border.

such as mammals [32]. By using synchrotron X-ray microtomography [33,34], we observed the bone growth lines in a suture of *C. croucheri* and showed that the convexities of sutures are areas with fast bone deposition when compared with the concavities (figure 6). Furthermore, we found a denser network of vascular canals in the concavities of the sutural borders when compared with the convexities, as we had previously observed in *Polypterus* and mice.

4. Discussion

Using a theoretical approach, we have demonstrated that external mechanical forces are sufficient to make a suture function in a way that reproduces many of the *in vivo* characteristics of sutural bone formation. The nature of the external stimulus we used in the simulations requires further discussion. From the analysis of the dispersion relation, it is clear that the outcome of the model was not influenced by the characteristics of the traction load (F). Namely, the final shape of the suture and the position of the bone forming regions did not depend on the fact that the force was quasi-static or periodic (with constant sign, i.e. always in traction). The results did not depend either on the amplitude of the traction F. This suggested that the continuous growth of the brain and cyclic stresses owing to mastication for instance could both induce bone deposition patterns leading to the appearance of interdigitations. One limitation of this study is the fact that the model cannot simulate the effects of compression. In fact, only fibre traction could transmit information to the sutural mesenchyme. Even though it is known that external compression cannot induce abnormal suture fusion [4], a model considering the effects of both compression and traction would be of interest, especially for the analysis of the fine effects of cyclic stresses such as mastication.

Suture interdigitations progressively develop complex patterns that diverge from the simple patterns produced by our model [10]. This fact could be the consequence of short simulation times (in accordance with the fact that we are essentially interested in early steps of suture formation; see the electronic supplementary material, file S1) but also owing to choice of constant mechanical coefficients (E_m, E_b and ν) and homogeneous haptotactic conditions within the mesenchyme (constant χ). With our set of hypotheses, the spatial and temporal scales of the patterns formed by the model were biologically realistic: the amplitude of the interdigitations reached approximately 2 mm in about 30 days of evolution. Interestingly, the time scale depended on the following parameters: χ, D and v_0. Longer simulation times and the introduction of heterogeneities may induce modifications in the outlines of the sutures produced by the model.

Interestingly, our hypothesis on the migration of cells from the mesenchyme towards the borders of the suture was supported by the fact that in the sagittal suture of mice, neural-crest-derived osteogenic cells from the mesenchyme progressively integrated into the mesoderm-derived parietal bones (see the electronic supplementary material, figure S3). The previously unknown central band of neural-crest-derived cells we observed at the centre of the mesenchyme of the sagittal sutures of adult mice (see the electronic supplementary material, figure S3) seemed to correspond to the quiescent mesenchyme core previously defined at earlier developmental stages [27]. In fact, such neural-crest-derived cell populations in the mesenchyme of the sagittal suture had already been described at the early stages of suture development (at E17.5 in mice embryos [35]), but their persistence at adult stages had not been observed. The presence of this population may be another sign in favour of the fact that sutures are active bone deposition sites during post-natal growth.

In a mouse mutant with defective mechanotransduction (the *Pkd2* mutant mouse), both the morphology of the sutures and the organization of their mesenchyme was abnormal. *Pkd* genes are known to play a role in mechanically induced bone formation in mice [13,30]. In this context, the abnormal sutures of the *Pkd2* mutant mouse can be interpreted as the result of a defect in the self-organization processes leading to normal suture patterning, owing to the lack of proper mechanotransduction required for collagen fibre rearrangement within

sutural mesenchyme. Further studies of the mechanisms of suture malformations in *Pkd* mutants will have to confirm this hypothesis.

By analysing the microscopic anatomy of sutures in a mammal, a basal actinopterygian and a placoderm, we provide evidence indicating that the mechanisms driving bone deposition in sutures share similarities between extinct ancestral vertebrates and extant mammals [36], and that a set of simple mechanotransduction phenomena may be conserved in all species presenting with dermal bones. In fact, placoderms are considered as the most basal jawed vertebrates and the state of a character within this group can be considered as plesiomorphic for all gnathostomes, including tetrapods [32]. From an evolutionary point of view, the dermal skeleton is the first-mineralized tissue appearing within jawed vertebrates. In this context, the mechanisms we described in our model are good candidates for being the ancestral set of events leading to bone formation in the first gnathostomes.

5. Conclusion

The model we propose simulates the morphological characteristics of vertebrate sutures by relying on simple mechanical processes. The limited number of crucial hypotheses we made (self-organization of collagen fibres in the mesenchyme directed by mechanical stress, mechanotransduction by migration of mesenchymal osteogenic cells along collagen fibres, subsequent bone deposition at the borders of the sutures) are corroborated by data from transgenic mice and high-resolution imaging in mice, rat and various fish samples.

Pattern formation involves a combination of chemical and physical processes. Our approach did not relate to any previous system producing interdigitated patterns but nevertheless simulated several fine biological characteristics of sutures (orientation of collagen fibres, appearance of interdigitations, specific distribution of bone deposition regions along the borders of the bone) via a previously unknown type of mechanically driven and biologically relevant instability. Most of the current research on suture maintenance and on craniosynostosis focuses on the molecular factors involved in bone proliferation and differentiation. The model we propose offers an initial theoretical basis that could be of use in the understanding of the interactions between bone deposition and physical processes. Our model illustrates the patterning ability of simple mechanical processes. Mechanotransduction could act upstream in several very common pathological situations such as deformational plagiocephalies or scaphocephaly, where there are striking and unexplained individual variations and differences in responses to external stimuli.

All experiments were approved by the UK Home Office.

We thank Raphael Bonnet, Cyril Charles, Mohamed Kahouadji, Emmanuel Pasco-Viel, Laurent Viriot and the ID19 beamline staff for assistance. We acknowledge Vincent Dupret from Uppsala University and Didier Geffard-Kuriyama for their help. We also thank Zerina Johanson and Jan Ove R. Ebbestad for lending us specimens in their care. All synchrotron scans were performed at the European Synchrotron Radiation Facility (projects nos EC203, EC519 and MD537). *Pkd2* mice were provided by Stefan Somlo. Special thanks to Catherine Choquet, Philippe Janvier, Abigael Tucker, Karen Liu, Jeremy Green, Gillian Morriss-Kay, Jacqueline Tabler, Triona Bolger and Susan Herring. R.H.K. is supported by King's College London and the Fondation Les Gueules Cassées. S.S. and P.A. are supported by the ERC Advanced Investigator grant no. 233111. Further support was also provided by ANR projects Maniphyc ANR-08-SYSC-010 and Rugo ANR-08-JCJC-0104-01 as well as funding from the European Union's Seventh Framework Programme (FP7-REGPOT-2009-1) under grant agreement no. 245749.

References

1. Rafferty KL, Herring SW, Marshall CD. 2003 Biomechanics of the rostrum and the role of facial sutures. *J. Morphol.* **257**, 33–44. (doi:10.1002/jmor.10104)
2. Opperman LA. 2000 Cranial sutures as intramembranous bone growth sites. *Dev. Dyn.* **219**, 472–485. (doi:10.1002/1097-0177(2000)9999:9999<::AID-DVDY1073>3.0.CO;2-F)
3. Rice DP. 2008 Clinical features of syndromic craniosynostosis. *Front. Oral Biol.* **12**, 91–106. (doi:10.1159/000115034)
4. Herring SW. 2008 Mechanical influences on suture development and patency. *Front. Oral Biol.* **12**, 41–56. (doi:10.1159/000115031)
5. Rice DP, Rice R. 2008 Locate, condense, differentiate, grow and confront: developmental mechanisms controlling intramembranous bone and suture formation and function. *Front. Oral Biol.* **12**, 22–40. (doi:10.1159/000115030)
6. Enlow DH. 1968 *The human face, an account of the postnatal growth and development of the craniofacial skeleton*. New York, NY: Harper and Row.
7. Byron CD, Borke J, Yu J, Pashley D, Wingard CJ, Hamrick M. 2004 Effects of increased muscle mass on mouse sagittal suture morphology and mechanics. *Anat. Rec. A* **279**, 676–684. (doi:10.1002/ar.a.20055)
8. Warren SM, Walder B, Dec W, Longaker MT, Ting K. 2008 Confocal laser scanning microscopic analysis of collagen scaffolding patterns in cranial sutures. *J. Craniofac. Surg.* **19**, 198–203. (doi:10.1097/scs.0b013e31815c8a9a)
9. Rice DP. 2008 Developmental anatomy of craniofacial sutures. *Front. Oral Biol.* **12**, 1–21. (doi:10.1159/000115028)
10. Miura T, Perlyn CA, Kinboshi M, Ogihara N, Kobayashi-Miura M, Morriss-Kay GM, Shiota K. 2009 Mechanisms of skull suture maintenance and interdigitation. *J. Anat.* **215**, 642–655. (doi:10.1111/j.1469-7580.2009.01148.x)
11. Sun Z, Lee E, Herring SW. 2004 Cranial sutures and bones: growth and fusion in relation to masticatory strain. *Anat. Rec. A* **276**, 150–161. (doi:10.1002/ar.a.20002)
12. Byron CD. 2006 Role of the osteoclast in cranial suture waveform patterning. *Anat. Rec. A* **288**, 552–563. (doi:10.1002/ar.a.20322)
13. Kolpakova-Hart E, McBratney-Owen B, Hou B, Fukai N, Nicolae C, Zhou J, Olsen BR. 2008 Growth of cranial synchondroses and sutures requires polycystin-1. *Dev. Biol.* **321**, 407–419. (doi:10.1016/j.ydbio.2008.07.005)
14. Turing AM. 1952 The chemical basis of morphogenesis. *Phil. Trans. R. Soc. Lond. B* **237**, 37–72. (doi:10.1098/rstb.1952.0012)
15. Hagberg A, Meron E. 1994 From labyrinthine patterns to spiral turbulence. *Phys. Rev. Lett.* **72**, 2495–2497. (doi:10.1103/PhysRevLett.72.2494)
16. Zollikofer CPE, Weissmann JD. 2011 A bidirectional interface growth model for cranial interosseous suture morphogenesis. *J. Anat.* **219**, 100–114. (doi:10.1111/j.1469-7580.2011.01386.x)
17. Sherratt JA, Martin P, Murray JD, Lewis J. 1992 Mathematical models of wound healing in embryonic and adult epidermis. *IMA J. Math. Appl. Med. Biol.* **9**, 177–196. (doi:10.1093/imammb/9.3.177)
18. Murray JD. 2003 *Mathematical biology. II. Spatial models and biomedical applications*. Berlin, Germany: Springer.
19. Jasinoski SC, Reddy BD, Louw KK, Chinsamy A. 2010 Mechanics of cranial sutures using the finite element method. *J. Biomech.* **43**, 3104–3111. (doi:10.1016/j.jbiomech.2010.08.007)
20. Spirli C, Okolicsanyi S, Fiorotto R, Fabris L, Cadamuro M, Lecchi S, Tian X, Somlo S,

Strazzabosco M. 2010 Erk1/2-dependent vascular endothelial growth factor signaling sustains cyst growth in polycystin-2 defective mice. *Gastroenterology* **138**, 360–371. (doi:10.1053/j.gastro.2009.09.005)

21. Soriano P. 1999 Generalized lacz expression with the ROSA26 Cre reporter strain. *Nat. Genet.* **21**, 70–71. (doi:10.1038/5007)
22. Chai Y, Jiang X, Ito Y, Bringas Jr. P, Han J, Rowitch DH, Soriano P, McMahon AP, Sucov HM. 2000 Fate of the mammalian cranial neural crest during tooth and mandibular morphogenesis. *Development* **127**, 1671–1679.
23. Popowics TE, Herring SW. 2007 Load transmission in the nasofrontal suture of the pig, *Sus scrofa*. *J. Biomech.* **40**, 837–844. (doi:10.1016/j.jbiomech.2006.03.011)
24. Peptan AI, Lopez A, Kopher RA, Mao JJ. 2008 Responses of intramembranous bone and sutures upon *in vivo* cyclic tensile and compressive loading. *Bone* **42**, 432–438. (doi:10.1016/j.bone.2007.05.014)
25. Iseki S, Wilkie AOM, Heath JK, Ishimaru T, Eto K, Morriss-Kay GM. 1997 Fgfr2 and osteopontin domains in the developing skull vault are mutually exclusive and can be altered by locally applied fgf2. *Development* **124**, 3375–3384.
26. Iseki S, Wilkie AOM, Morriss-Kay GM. 1999 Fgfr1 and fgfr2 have distinct differentiation- and proliferation-related roles in the developing mouse skull vault. *Development* **126**, 5611–5620.
27. Lana-Elola E, Rice R, Grigoriadis AE, Rice DPC. 2007 Cell fate specification during calvarial bone and suture development. *Dev. Biol.* **311**, 335–346. (doi:10.1016/j.ydbio.2007.08.028)
28. Chandrasekhar S. 1961 *Hydrodynamic and hydromagnetic stability*. Gloucestershire, UK: Clarendon Press.
29. Fedkiw R, Osher S. 2002 *Level set methods and dynamic implicit surfaces*. Berlin, Germany: Springer.
30. Xiao Z, Dallas M, Qiu N, Nicolella D, Cao L, Johnson M, Bonewald L, Quarles LD. 2011 Conditional deletion of Pkd1 in osteocytes disrupts skeletal mechanosensing in mice. *FASEB J.* **25**, 2418–2432. (doi:10.1096/fj.10-180299)
31. Gardiner BG, Miles RS. 1994 *Eubrachythoracid arthrodires* from Gogo, Western Australia. *Zool. J. Linn. Soc.* **112**, 443–477. (doi:10.1111/j.1096-3642.1994.tb00331.x)
32. Janvier P. 1996 *Early vertebrates*. Alderly, UK: Clarendon Press.
33. Tafforeau P, Smith TM. 2008 Nondestructive imaging of hominoid dental microstructure using phase contrast X-ray synchrotron microtomography. *J. Hum. Evol.* **54**, 272–278. (doi:10.1016/j.jhevol.2007.09.018)
34. Sanchez S, Ahlberg PE, Trinajstic K, Mirone A, Tafforeau P. 2012 Three dimensional synchrotron virtual paleohistology: a new insight into the world of fossil bone microstructures. *Microsc. Microanal. J. Hum. Evol.* **18**, 1095–1105. (doi:10.1017/S1431927612001079)
35. Jiang X, Iseki S, Maxson RE, Sucov HM, Morriss-Kay GM. 2002 Tissue origins and interactions in the mammalian skull vault. *Dev. Biol.* **241**, 106–116. (doi:10.1006/dbio.2001.0487)
36. Downs JP, Donoghue CJ. 2009 Skeletal histology of *Bothriolepis canadensis* (placodermi, antiarchi) and evolution of the skeleton at the origin of the jawed vertebrates. *J. Morphol.* **270**, 1364–1380. (doi:10.1002/jmor.10765)